Unsteady analyses of thermal glass fibre drawing processes

M. GREGORY FOREST [1] and HONG ZHOU [2]

[1] *Department of Mathematics, University of North Carolina, Chapel Hill, NC 27599-3250, USA*
[2] *Department of Mathematics, University of California, Santa Cruz, CA 95064, USA*

Fibre drawing is an important industrial process for synthetic polymers and optical communications. In the manufacture of optical fibres, precise diameter control is critical to waveguide performance, with tolerances in the submicron range that are met through feedback controls on processing conditions. Fluctuations arise from material non-uniformity plague synthetic polymers but not optical silicate fibres which are drawn from a pristine source. The steady drawing process for glass fibres is well-understood (e.g. [11, 12, 20]). The linearized stability of steady solutions, which characterize limits on draw speed versus processing and material properties, is well-understood (e.g. [9, 10, 11]). Feedback is inherently transient, whereby one adjusts processing conditions in real time based on observations of diameter variations. Our goal in this paper is to delineate the degree of sensitivity to transient fluctuations in processing boundary conditions, for thermal glass fibre steady states that are linearly stable. This is the relevant information for identifying potential sources of observed diameter fluctuation, and for designing the boundary controls necessary to alter existing diameter variations. To evaluate the time-dependent final diameter response to boundary fluctuations, we numerically solve the model nonlinear partial differential equations of thermal glass fibre processing. Our model simulations indicate a relative insensitivity to mechanical effects (such as take-up rates, feed-in rates), but strong sensitivity to thermal fluctuations, which typically form a basis for feedback control.

1 Introduction

In the early 1960s, Corning's development of optical fibres with extremely low attenuation, on the order of decibels per kilometer, opened the door to wideband communication signal transmission. Optical fibre is drawn from a silica preform, typically 10–25 mm in diameter and 60–100 cm in length, yielding continuous lengths of as much as 40–300 km [26].

Fibre drawing (Figure 1) involves a heat source at the tip of the preform which melts the glass, allowing it to flow downward while shrinking in diameter and cooling, reaching approximately 100 microns at solidification. The upstream fibre velocity range is 0.002–0.03 cm/s, depending on the heat source, preform diameter, and draw speed (the imposed downstream velocity past the solidification location). Silicates have relatively high softening temperatures which require heat sources in the range of 1950–2250°C. A pulling and winding mechanism sustains a drawing force.

In the manufacture of optical fibres, precise diameter control is critical to waveguide
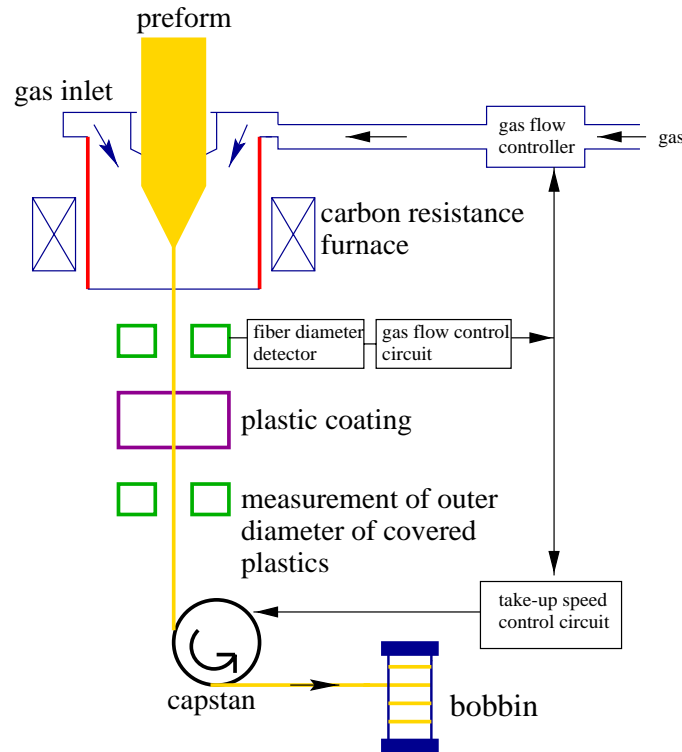
FIGURE 1. Fibre drawing using gas flow rate control.

performance. Synthetic polymeric fibres are used primarily for bulk performance properties, so processes are pushed near the limit of stable draw ratios (the ratio of axial velocities at the upstream and downstream locations). Optical fibres are individually important, and processes are run well within the stable operating regime; standard literature issues of instability phenomena such as draw resonance [21] are not relevant for optical fibres. Signal propagation in optical fibres [19] has revealed that diameter variations should be within 1% of the nominal diameter in order to minimize transmission losses. Fibre asymmetry is another source of additional complexity in optical pulse transmission, leading to coupling of the two polarization modes that would otherwise propagate independently for axisymmetric fibres; this effect is not addressed here. To suppress variations, the fibre diameter is monitored continuously and then sophisticated feedback controls are employed on both temperature and mechanical operating conditions. Mathematically, the feedback consists of time-dependent variations of steady boundary conditions. Small variations are presumed to arise from uncontrolled transient fluctuations in the identical process conditions one subsequently controls. Thus the desire for accurate models which yield the cause and effect relationship of transient fluctuations in the regime of stable steady state fibre drawing processes.

The drawing of glass fibres has been modelled by many authors, for example, Glicksman [12], Burgman [1], Geyling & Homsy [11], Huynh & Tanner [14], and Dewynne, Ockendon & Wilmott [5].

Early studies focused on steady solutions, followed later by analysis of linearized stability of steady isothermal fibre processes. The extension of stability to include the liquid-solid phase transition is provided in Forest *et al.* [9], with many references to the previous literature. We underscore the delicate tolerances on optical fibres because it shifts the mathematical focus beyond linearized stability to the next level of sophistication, in particular beyond analytical treatment. Optical fibre processes operate in highly stable regimes, removed from any incipient instabilities from the hydrodynamics or thermodynamics. The sub-micron fluctuations that are the target of current control mechanisms can only be addressed by a full transient model and simulation. In this manner, one can quantify all potential mechanisms and sources of diameter variations. Myers [20] has done some nice work in this direction, which we aim to extend here. We first construct a realistic model for optical fibres, a straightforward generalization of Geyling & Homsy [11] to include inertial, gravitational, and capillary effects. We then develop an efficient second-order numerical method based on flux limiting [16] and a MacCormack scheme [18] to solve the thermal optical fibre model equations.

The main focus of this paper is to study the sensitivity of the process to small disturbances injected through time-dependent boundary conditions, which are precisely the available control conditions. The preliminary step of a steady boundary-value solver is straightforward [9, 11], so we proceed directly to the PDE simulations. We further note that the parameter regimes and steady boundary conditions are well within the stability range of this model. In Forest *et al.* [9], we benchmark the linearized stability analysis against the full PDE time-dependent code, in a more general model that reduces to this one for viscous thermal fluids.

2 The equations of motion

In the glass fibre preform drawing process, fibres are produced by applying tension to the bottom of a glass rod as it is lowered into a furnace. Models of viscous draw-down flows are typically based on a *quasi-one-dimensional* approximation in which the nondimensionalized *free surface radius* ϕ, *axial velocity* v, and *temperature* T are homogeneous in the radial direction and depend only on the axial coordinate z and time t. These models offer an alternative to industrial-strength codes for the full 3D, free surface equations. A representative historical reference list is provided in the references.

The leading order, non-dimensional, *quasi-1D model equations* for axisymmetric filaments consist of the continuity, momentum balance and energy equations:

$$\begin{cases} (\phi^2)_t + (v\phi^2)_z = 0, \\ (\phi^2 v)_t + (\phi^2 v^2)_z = \frac{1}{F}\phi^2 + \frac{1}{W}\phi_z + [\phi^2 \eta(T) v_z]_z, \\ \phi^2(T_t + v T_z) = H\,\phi\,(T_{wall}^4 - T^4) - 2\,St\,(v\phi)^m\,(T - T_a), \end{cases} \tag{2.1}$$

where $z \in [0, 1]$, and the temperature-dependent dimensionless viscosity $\eta(T)$ is

$$\eta(T) = \exp\left[\alpha\left(\frac{1}{T} - \beta\right)\right]. \tag{2.2}$$

The choice of scales and definitions of all parameters are given in Appendix A. *F*

and W are the Froude and Weber numbers, which respectively parametrize gravity and surface tension relative to inertia; St is the Stanton number, which is the dimensionless heat transfer coefficient, and the term $(v\phi)^m$ is an empirical heat transfer correlation developed in the textile fibre industry [15]. We employ the value $m = 1/3$ as in Geyling & Homsy [11]. H is the effective radiative transfer coefficient for the surface of the fibre; T_{wall} is the temperature of the furnace; T_a is the ambient air temperature. The radiative heat transfer effect is specific to glasses; see Myers [20] for a detailed discussion. The furnace temperature T_{wall} may vary in the axial direction. One can also use a nonconstant ambient temperature T_a to simulate heating and cooling zones. In this paper, for simplicity, we treat both T_{wall} and T_a as constants. A detailed model for radiative heat transfer can be found in Myers [20]. Typical values of these parameters are given in Appendix A.

The dimensionless boundary conditions are specified as follows:

- Upstream boundary conditions:

$$\phi(0) = 1, v(0) = 1, T(0) = 1.$$

- Downstream boundary conditions:

$$v(1) = Dr \,(\text{draw ratio}).$$

Let

$$\mathbf{w} = \begin{bmatrix} \phi^2 \\ \phi^2 v \\ T \end{bmatrix}, \tag{2.3}$$

then (2.1) can be put in a general form

$$\mathbf{w}_t = -A(\mathbf{w})\mathbf{w}_z + M(\mathbf{w}) + N(\mathbf{w}_z) + [G(\mathbf{w})\mathbf{w}_z]_z, \tag{2.4}$$

where

$$A(\mathbf{w}) = \begin{bmatrix} 0 & 1 & 0 \\ -v^2 - \frac{1}{2W\phi} & 2v & 0 \\ 0 & 0 & v \end{bmatrix}, \tag{2.5}$$

and $N(\mathbf{w}_z)$, $M(\mathbf{w})$, $G(\mathbf{w})$ are easily constructed from (2.1). The three eigenvalues of the transport matrix A are

$$\lambda = v \pm \sqrt{-\frac{1}{2W\phi}}, \, v. \tag{2.6}$$

Therefore, the system (2.1) is a second-order PDE, whose first two equations would form an elliptic system if viscosity were ignored. This Hadamard behavior is the result of the longwave asymptotic approximation on the surface tension/curvature terms in the boundary conditions of the free surface [2, 7, 24]. The viscous terms are necessary to regularize the model system.

In glass fibres the capillary instability is strongest near the preform tip, and then weakens downstream as the glass cools. Most treatments ignore capillary effects on two premises: the effect is weak relative to viscosity and thermal effects; and it presents significant numerical difficulties. The latter nuisance we dispel below with an efficient numerical scheme to handle these terms. The first issue is one we have to grapple with. Since the

entire motivation of this model is to assert the source of small diameter fluctuations, we are compelled to resolve any source of transient amplification of perturbations that arise in the process, especially if they may be subtle.

If $T_{wall} = T_a$ and $1/F = 0$ (no gravity), the system (2.1) admits a simple constant solution $\mathbf{w}_0 = (\phi_0^2, \phi_0^2 v_0, T_a)$. A linearized stability analysis, assuming $\mathbf{w} = \mathbf{w}_0 + \delta \mathbf{w}_1 e^{ikz+qt}$, yields the dispersion relation

$$Re(q_1(k)) = -\frac{\eta(T_a)k^2}{2} + \sqrt{\left(\frac{\eta(T_a)k^2}{2}\right)^2 + \frac{k^2}{2W\phi_0}} > 0,$$

$$Re(q_2(k)) = -\frac{\eta(T_a)k^2}{2} - \sqrt{\left(\frac{\eta(T_a)k^2}{2}\right)^2 + \frac{k^2}{2W\phi_0}} < 0, \qquad (2.7)$$

$$Re(q_3(k)) = -\frac{4HT_0^3}{\phi_0} - \frac{2St(\phi_0 v_0)^m}{\phi_0^2} < 0.$$

The linearized growth rate $Re(q_1(k))$ is uniformly bounded by

$$Re(q_1(k)) \leqslant \frac{1}{2W\phi_0\eta(T_a)}, \qquad (2.8)$$

which implies that the 1D nonlinear asymptotic equations (2.1) are locally well-posed as an evolutionary system. We underscore this simple analysis is to exhibit local well-posedness of the model equations, but it is not relevant to stability of steady fibre solutions which satisfy a two-point boundary value problem. Capillary effects compete in these processes, but the classical Rayleigh instability is buried in the analysis of the linearization of that very different linearized, variable coefficient, system.

If one assumes that viscosity dominates and thereby ignores the effects of fluid inertia, surface tension, and gravity, then the system (2.1) is reduced to (set $m = 1/3$)

$$(\phi^2)_t + (v\phi^2)_z = 0, \qquad (2.9)$$

$$\left[\phi^2\eta(T)v_z\right]_z = 0, \qquad (2.10)$$

$$T_t + vT_z = \frac{H}{\phi}(T_{wall}^4 - T^4) - 2St\frac{1}{\phi^{5/3}}v^{1/3}(T - T_a), \qquad (2.11)$$

whose steady state solutions and their linearized stability have been studied by Geyling & Homsy [11]. Dewynne, Ockendon & Wilmott [5] also studied this reduced model, where the energy equation (2.11) is not included but the viscosity η is posited as a function of z or t only. Under these assumptions, they derive exact solutions.

In this paper our main focus is the numerical study of process sensitivities based on the model (2.1). A brief description of the numerical method is given in Appendix B.

3 Unsteady optical glass fibre drawing

The excellent monograph of Pearson [21, Ch. 15] contains a discussion of various approaches to unsteady fibre processes. We reiterate that the issue of relevance here is the sensitivity of stable steady state solutions to unsteady boundary data. First, we calculate the steady state solution of (2.1) using a boundary-value solver described in Forest *et al.* [9]. Figure 2 depicts the solution for $1/F = 0.0127$, $1/W = 2.4$, $H = 0.2$, $St = 0.2$,
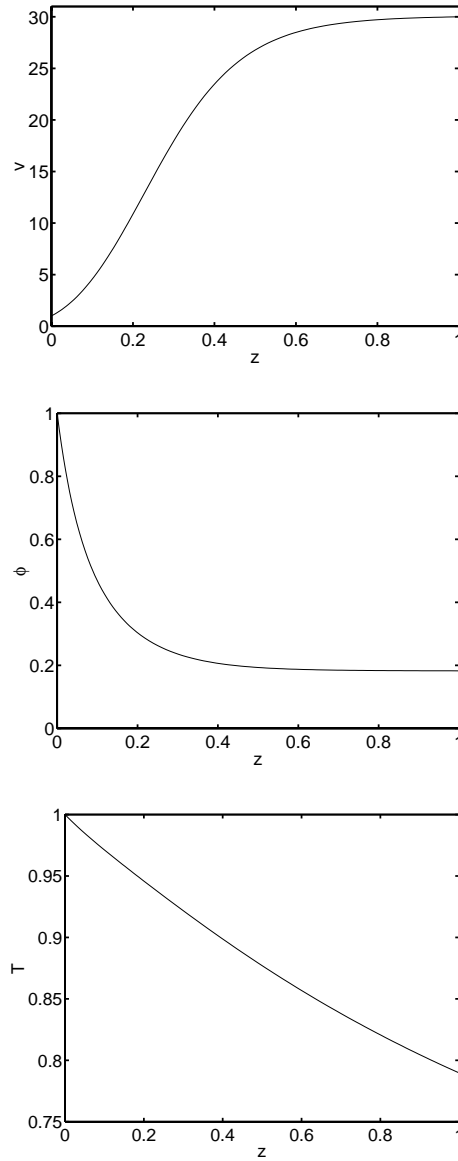
FIGURE 2. The steady state solution of (2.1) where $1/F = 0.0127$, $1/W = 2.4$, $H = 0.2$, $St = 0.2$,
$\alpha = 30$, $\beta = 1.0113$, $T_a = 0.6$, $T_{wall} = 0.6$, $Dr = 30$.

$\alpha = 30$, $\beta = 1.0113$, $T_a = T_{wall} = 0.6$, $m = 1/3$, and $Dr = 30$. This is a typical parameter regime, deduced in Appendix A from literature data. We have confirmed stability of steady states in a wide parameter neighbourhood of this particular steady state, both with respect to linearized stability and through full numerical simulation of the nonlinear equations. Thus, the steady state process is stable to superimposed spatial perturbations.

We next assess the effects of transient fluctuations in each process boundary condition: take-up rate, preform tip rate, tip diameter and tip temperature. These are the operating conditions from which one can design controls. We will present *relative quantities* only,
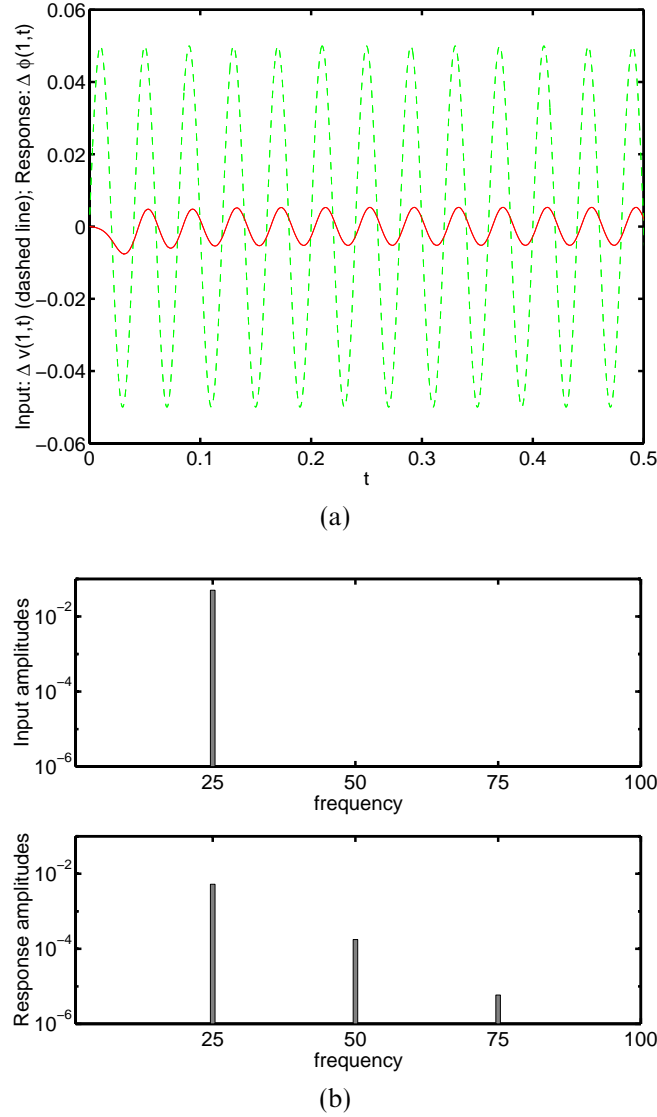
FIGURE 3. Take-up rate fluctuations. (a) The imposed take-up velocity perturbation, $\Delta v(1, t)$ (dashed) and the fibre radius response, $\Delta \phi(1, t)$ (solid). (b) The discrete Fourier transforms of 3(a).

which allow us to view all input and response functions on the same scale. More specifically, we will investigate the response of $\Delta \phi(1, t)$ to $\Delta v(1, t)$, $\Delta v(0, t)$, $\Delta \phi(0, t)$ and $\Delta T(0, t)$ respectively, where

$$\Delta \phi(1, t) = \frac{\phi(1, t) - \phi(1)}{\phi(1)}, \quad \Delta v(1, t) = \frac{v(1, t) - v(1)}{v(1)},$$

$$\Delta v(0, t) = \frac{v(0, t) - v(0)}{v(0)}, \quad \Delta T(0, t) = \frac{T(0, t) - T(0)}{T(0)}, \tag{3.1}$$

and $v(1)$, $v(0)$, $\phi(0)$, $T(0)$ are the steady state boundary conditions.
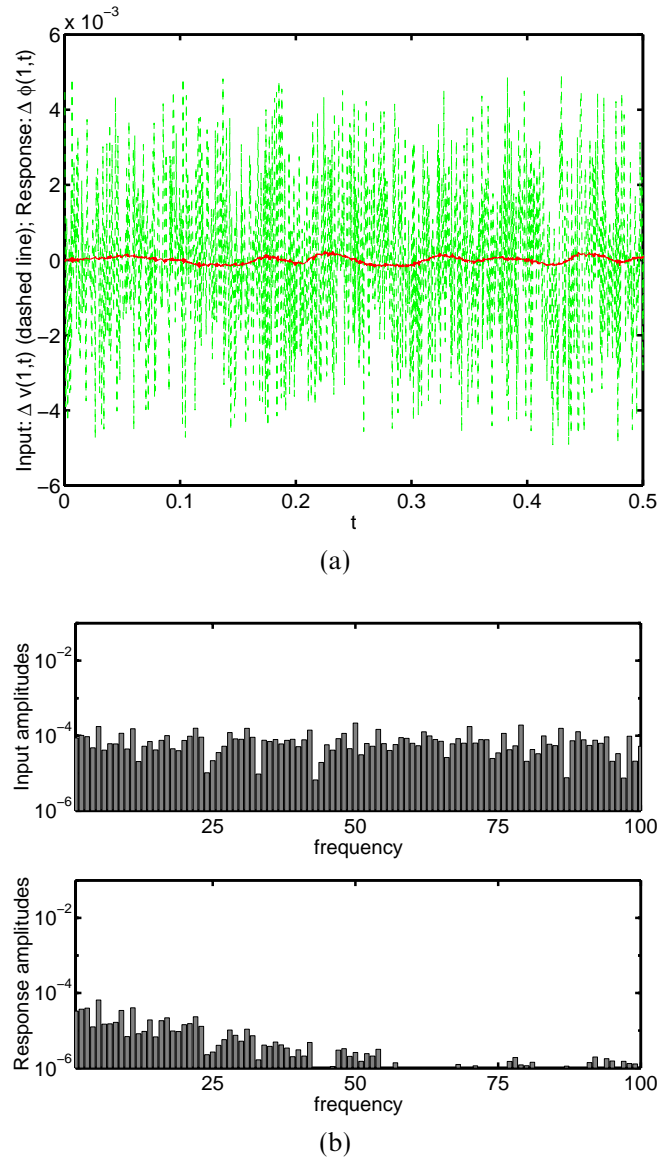
FIGURE 4. Take-up rate fluctuations: random input. (a) Relative final fibre radius response (solid) to a random fluctuation in the take-up speed of the fibre (dashed). (b) The Fourier spectrum of 4(a).

Take-up rate fluctuations

To study the effect of unsteady take-up rates, we perturb the constant take-up speed, $v(1)$, at a fixed frequency (ω) and amplitude (a):

$$v(1, t) = v(1)[1 + a \sin(2\pi\omega t)]. \tag{3.2}$$

In Figure 3(a) we show the relative radius response, $\Delta\phi(1, t)$, to a single-frequency perturbation (3.2) with $\omega = 25$ and $a = 5\%$. Figure 3(b) shows the corresponding power spectrum of Figure 3(a), which indicates that the dominant perturbation frequency of the
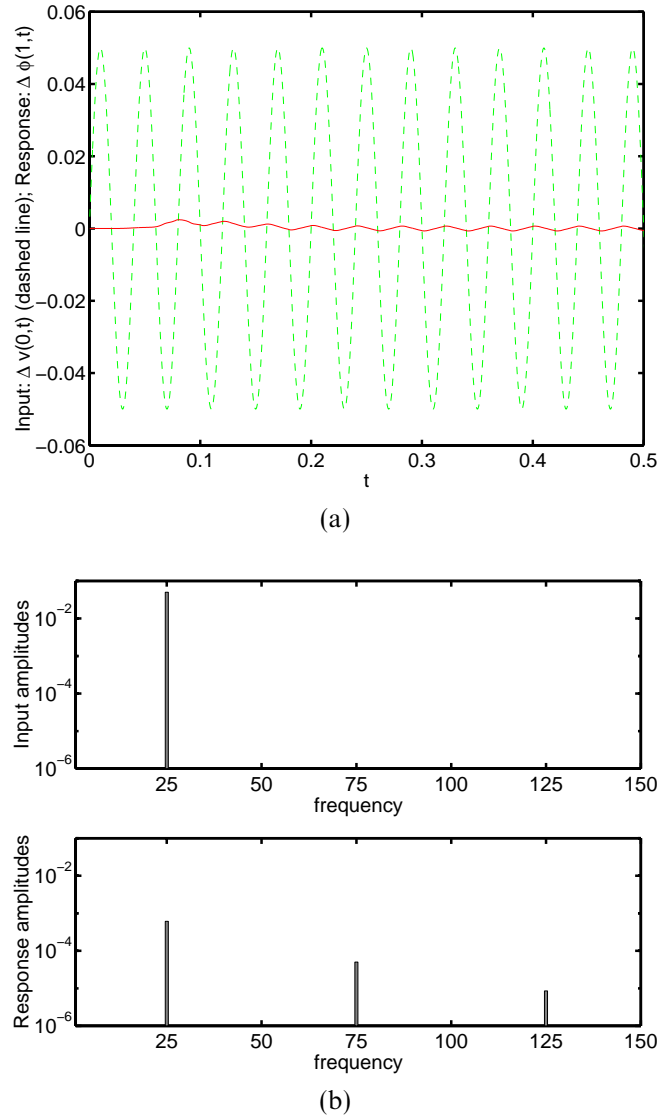
(a)

(b)

FIGURE 5. Tip rate fluctuations. (a) Relative final fibre radius response (solid) to a periodic, single-frequency fluctuation of the velocity at the preform (dashed). (b) The discrete Fourier spectrum of 5(a).

response $\Delta\phi(1,t)$ matches the input frequency of $\Delta v(1,t)$. Due to nonlinearity, sideband frequencies of $\Delta\phi(1,t)$ also occur but with very small amplitudes. Figure 3 demonstrates that the draw-down flow is insensitive to unsteady take-up rates. A 5% relative take-up velocity perturbation produces a final relative diameter variation of 0.5%. Notice that the fibre response is nonuniform at first, then the envelope equilibrates.

Figure 4 depicts the fibre diameter response to a random fluctuation of $v(1,t)$. Note the decay of the response amplitudes in the high frequency regime.
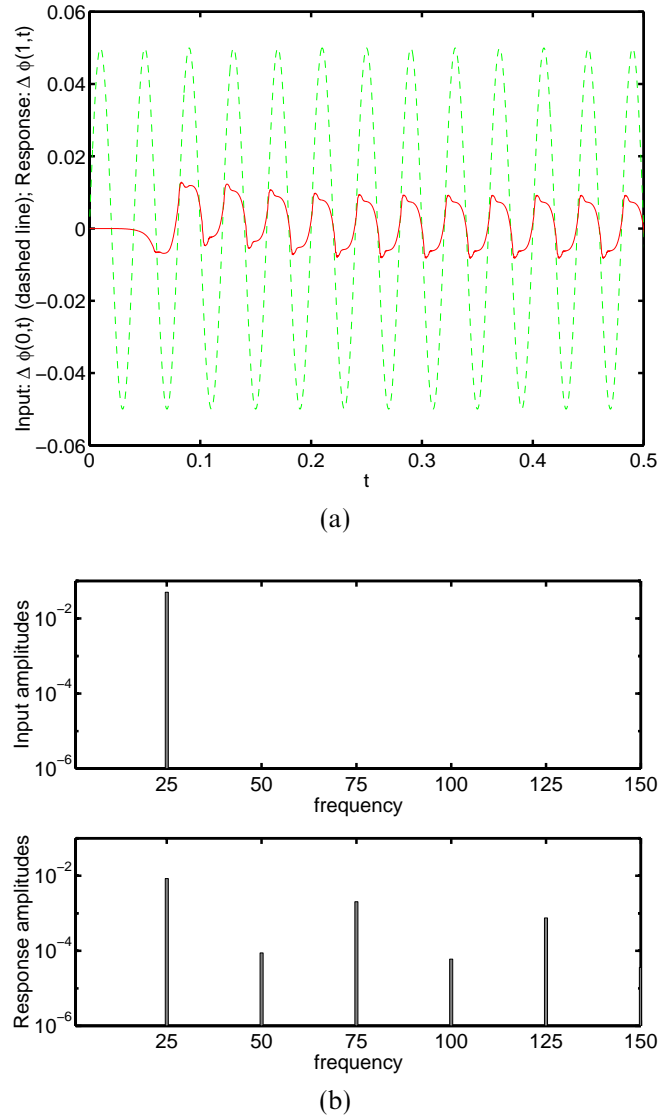
FIGURE 6. Tip diameter fluctuations. (a) Relative final fibre radius response (solid) to a periodic, single-frequency fluctuation of the fibre radius at the preform (dashed). (b) The discrete Fourier spectrum of 6(a).

Tip rate fluctuations

We now consider a perturbed tip rate in the form

$$v(0, t) = v(0)[1 + a \sin(2 \pi \omega t)]. \tag{3.3}$$

In Figure 5 we show the response of the draw-down flow to the perturbation of feed-in rate (3.3) with $\omega = 25$, $a = 0.05$. Our results indicate that the effect of unsteady feed-in rates on draw-down flow is insignificant: a 5% input variation yields a 0.2% response.
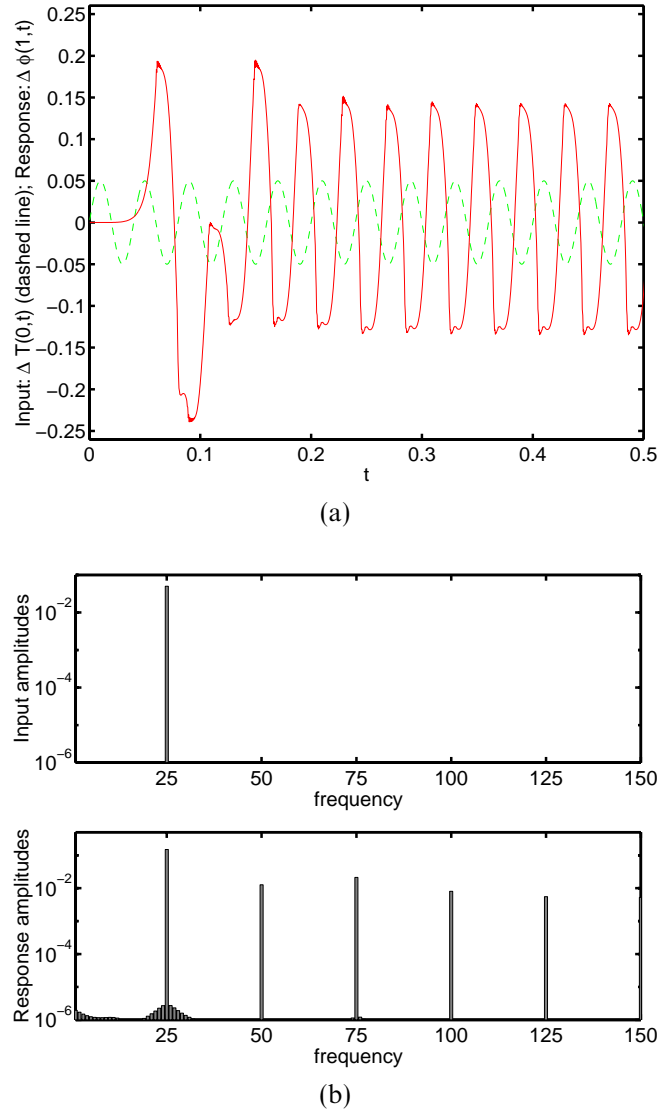
FIGURE 7. Tip temperature fluctuations. (a) Relative final fibre radius response (solid) to a periodic, single-frequency fluctuation of the fibre temperature at the preform (dashed). (b) The discrete Fourier spectrum of 7(a).

Tip diameter fluctuations

Consider a perturbed tip radius

$$\phi(0,t) = \phi(0)[1 + a \sin(2\pi\omega t)]. \tag{3.4}$$

Figure 6 depicts the response of take-up radius to the perturbations of feed-in radius $\phi(0,t)$ where $a = 0.05$, $\omega = 25$. These figures show that the diameter is likewise insensitive to the unsteady feed-in radius $\phi(0,t)$: a 5% input variation yields around a 1% response.
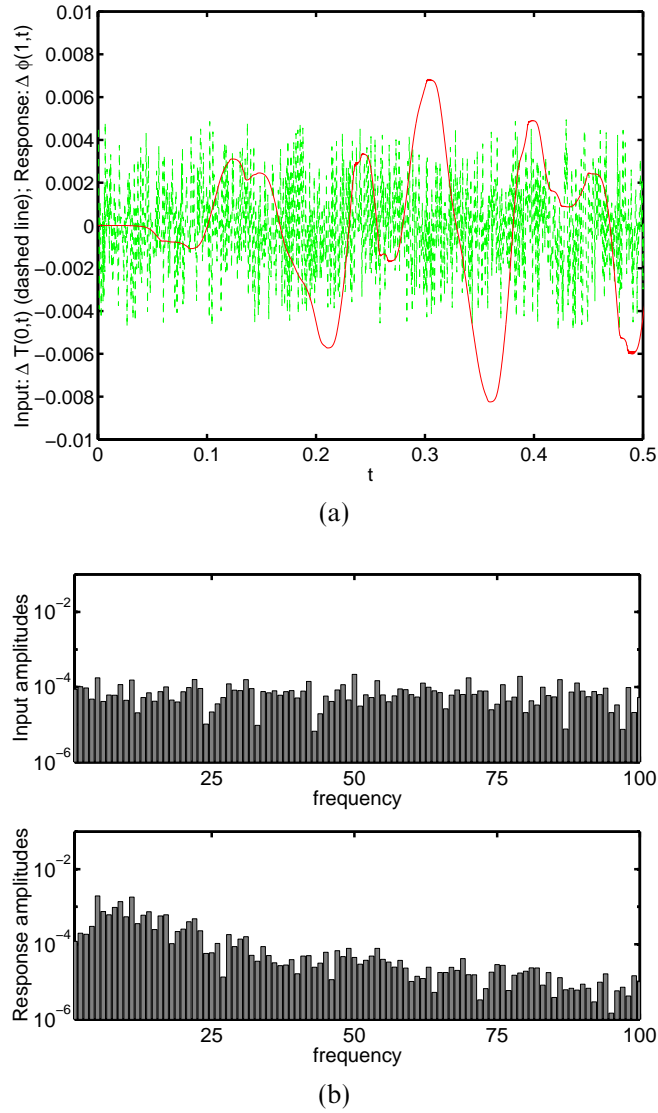
(a)

(b)

FIGURE 8. Tip temperature fluctuations. (a) Final fibre radius response (solid) to a random fluctuation of the fibre temperature at the preform (dashed). (b) The discrete Fourier spectrum of 8(a).

Tip temperature fluctuations

Consider

$$T(0, t) = T(0)[1 + a \sin(2\pi\omega t)]. \tag{3.5}$$

In Figure 7 we display the effect of the perturbations (3.5) with $a = 0.05$, $\omega = 25$. Clearly, the effect is significant: a 5% tip temperature relative variation is amplified into a 10% relative variation in the fibre diameter. Figure 8 shows the diameter response to a random tip temperature perturbation.
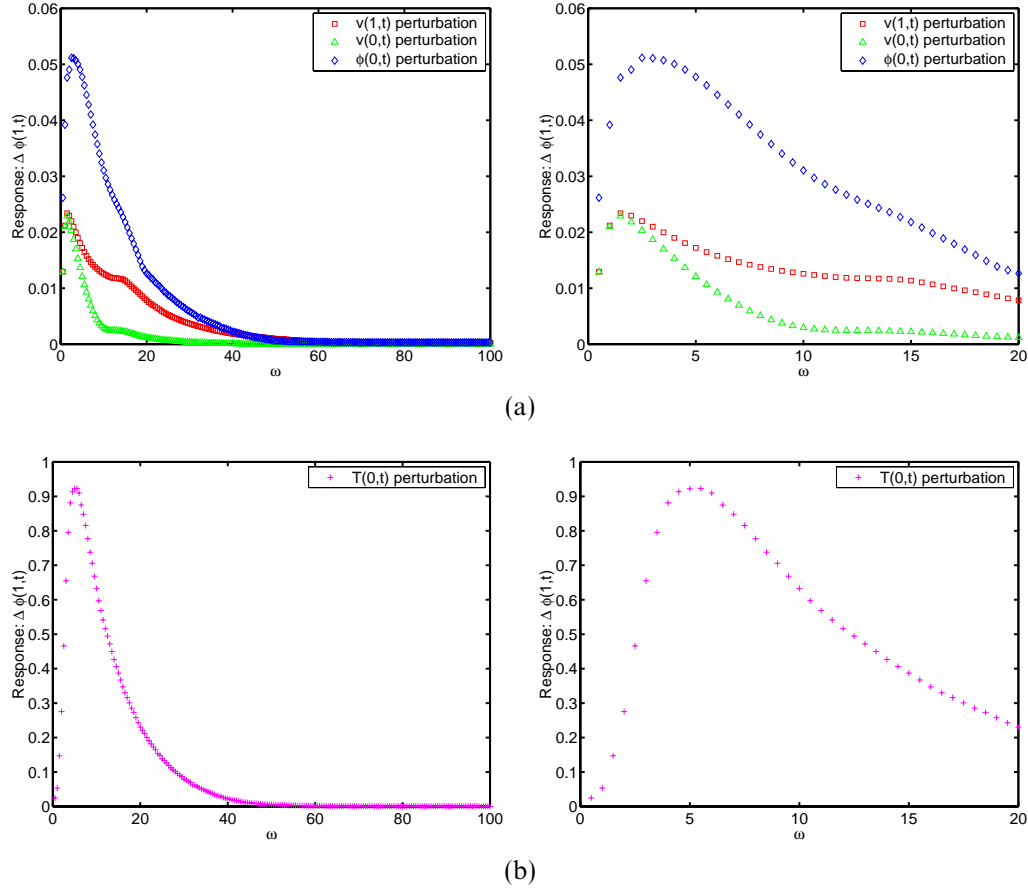
(a)

(b)

FIGURE 9. Relative final radius response vs. input frequency for all boundary perturbations. The input variations each have amplitude .05.

Diameter response curves vs. input frequency for all time-dependent boundary data

Finally, we move from *single solutions* to a summary in Figure 9 of the relative diameter response to all frequencies for each available input function, (3.2)–(3.5). The relative perturbation amplitude is fixed, $a = 0.05$. Note that the diameter response is not monotone; there is a peak frequency that induces maximum response. Myers [20] has obtained similar results for the frequency response to a periodic take-up rate. Our results indicate that diameter variability due to temperature rate fluctuations dominates any effects due to mechanical process fluctuations.

4 Conclusions

This paper provides an unsteady simulation of thermal glass fibre drawing processes. Our numerical method combines the MacCormack scheme from hyperbolic conservation laws with the ideas of flux limiting generally used in high resolution methods [13]. We simulate transient perturbations at boundaries, which are the primary source of fibre nonuniformities and which are unresolved by linearized stability analyses (e.g. [9, 10, 11,

15, 17]). We find that thermal boundary fluctuations are the dominant influence on fibre diameter, whereas mechanical effects are less significant, consistent with experimental observations for polymeric fibres [25]. These results imply that an isothermal model, or a model which posits a temperature profile and thereby suppresses feedback between the fibre kinematics and energy equation, can not resolve the dominant mechanism for fibre diameter fluctuations.

Acknowledgement and Disclaimer

Appendix A Non-dimensional parameters

Recall the typical scales are t_0, z_0, r_0, T_0, which are the characteristic time, axial length scale, transverse length scale and temperature, respectively. From these characteristic scales, the following dimensionless parameters are defined:

$$F = \frac{z_0}{g t_0^2}, \quad W = \frac{\rho r_0 z_0^2}{\sigma t_0^2},$$
$$H = \frac{z_0 \kappa_{sb} \delta T_0^3}{\rho v_0 c_p r_0}, \quad St = \frac{h z_0}{\rho c_p r_0 v_0}, \tag{A 1}$$

where g is the gravity, σ is the surface tension coefficient, ρ is the fluid density, c_p is the specific heat, κ_{sb} is the Stefan-Boltzmann constant, δ is an effective emissivity at the surface, h is the heat transfer coefficient.

According to Geyling & Homsy [11], typical values for St lie between 0.02 and 0.2; typical values for the radiative transfer coefficient H are between 0.1 and 2.0; the values for α, β are also adopted from Geyling & Homsy [11]; the choices for F, W are based on Forest *et al.* [10].

Appendix B The numerical method

We implement the MacCormack method [18] with flux limiting [16], together with the predictor-corrector method, to solve the glass fibre equations (2.1).

MacCormack's scheme [18] was originally developed for conservative hyperbolic equations. First it uses an one-sided upwind-type step to obtain predicted values, followed by staggered two-level differences to approximate the spatial derivatives. Staggering refers to the choices: in the first level the upwind-type stencil is employed, whereas in the second level the downwind-type stencil is used with the predictor values. We then introduce flux

limiting to control small scale oscillations. Numerical small scale oscillations are physically unacceptable: the slender model equations (2.1) are valid only for $O(1)$ wavelengths in this dimensionless coordinate z. Numerical generation of short wavelengths violates the validity of the equations. The inclusion of flux limiting controls numerical oscillations and thereby maintains model consistency.

For glass fibres, the viscosity is very large, especially as the fibre cools. We find the Crank–Nicolson method does not yield unconditional stability for very large viscosities. By saying this, we mean that the time step cannot simply be controlled by the CFL condition. To see this intuitively, consider the ODE

$$y' = -\lambda y. \tag{B 1}$$

The amplification factor $\rho(\lambda)$ of the Crank–Nicolson method is

$$\rho(\lambda) = \frac{1 - \frac{\lambda}{2}\Delta t}{1 + \frac{\lambda}{2}\Delta t}, \tag{B 2}$$

and $|\rho(\lambda)| \to 1$ when $\lambda \Delta t >> 1$.

To overcome this stability problem, one can use a weighting scheme in the corrector step, as employed by Eggers & Dupont [6] for the isothermal limit of this model.

Introducing $u = \phi^2$, $w = \phi^2 v$, we rewrite (2.1) as

$$\begin{cases} u_t + w_z = 0, \\ w_t + \left(\dfrac{w^2}{u} - \dfrac{1}{W}\sqrt{u}\right)_z = \dfrac{1}{F}u + \left[\eta(T)u(\dfrac{w}{u})_z\right]_z, \\ T_t + \dfrac{w}{u}T_z = \dfrac{H}{\sqrt{u}}(T_{wall}^4 - T^4) - \dfrac{2\,St}{u}\left[\left(\dfrac{w}{\sqrt{u}}\right)^m\right](T - T_a). \end{cases} \tag{B 3}$$

Divide time into intervals of length Δt and let $\Delta z = 1/N$ be the spatial increment. Let ϕ_j^n approximate the solution $\phi(j\Delta z, n\Delta t)$ and v_j^n approximate the solution $v(j\Delta z, n\Delta t)$. The numerical scheme consists of two steps.

In the first step (e.g. predictor step), for $j = 2, \cdots, N$, one has

$$u_j^* = u_j^n - \frac{\Delta t}{\Delta z}\left(f_{j+\frac{1}{2}} - f_{j-\frac{1}{2}}\right), \tag{B 4}$$

$$\begin{aligned} w_j^* = w_j^n &- \frac{\Delta t}{\Delta z}(g_{j+\frac{1}{2}} - g_{j-\frac{1}{2}}) + \frac{\Delta t}{F}u_j^n \\ &+ \frac{\Delta t}{(\Delta z)^2}\left[\eta\left(\frac{T_{j+1}^n + T_j^n}{2}\right)\frac{u_{j+1}^n + u_j^n}{2}\left(\frac{w_{j+1}^*}{u_{j+1}^n} - \frac{w_j^*}{u_j^n}\right)\right. \\ &\left.- \eta\left(\frac{T_j^n + T_{j-1}^n}{2}\right)\frac{u_j^n + u_{j-1}^n}{2}\left(\frac{w_j^*}{u_j^n} - \frac{w_{j-1}^*}{u_{j-1}^n}\right)\right], \end{aligned} \tag{B 5}$$

$$\begin{aligned} T_j^* = T_j^n &- \frac{\Delta t}{\Delta z}\frac{w_j^n}{u_j^n}(T_j^n - T_{j-1}^n) + \frac{H}{\sqrt{u_j^n}}[T_{wall}^4 - (T_j^n)^4]\Delta t \\ &- \frac{2\,St}{u_j^n}\left[\frac{w_j^n}{\sqrt{u_j^n}}\right]^m(T_j^n - T_a)\Delta t, \end{aligned} \tag{B 6}$$

where the flux functions are

$$f_{j+\frac{1}{2}} = w_j^n, \tag{B 7}$$

$$g_{j+\frac{1}{2}} = \frac{[w_j^n]^2}{u_j^n} - \frac{1}{W}\sqrt{u_j^n}. \tag{B 8}$$

The boundary conditions are:

$$\text{upstream: } u_1^n, w_1^n, T_1^n \text{ are given.} \tag{B 9}$$

$$\text{downstream:} \begin{cases} \dfrac{w_{N+1}^n}{u_{N+1}^n} \equiv Dr \text{ is given,} \\[2mm] w_{N+1}^n = 2w_N^n - w_{N-1}^n, \\[2mm] u_{N+1}^n = w_{N+1}^n/Dr, \\[2mm] T_{N+1}^n = 2T_N^n - T_{N-1}^n. \end{cases} \tag{B 10}$$

In the second step (e.g. corrector step), we will update w first and then use the new values of w other than the predicted values of w to update u. This treatment seems more natural. Therefore, for $j = 2, \cdots, N$, we have

$$u_j^{n+1} = u_j^n - \frac{\Delta t}{\Delta z}(\tilde{f}_{j+\frac{1}{2}} - \tilde{f}_{j-\frac{1}{2}}), \tag{B 11}$$

$$\begin{aligned} w_j^{n+1} = w_j^n &- \frac{\Delta t}{\Delta z}(\tilde{g}_{j+\frac{1}{2}} - \tilde{g}_{j-\frac{1}{2}}) + \frac{\Delta t}{2F}(u_j^n + u_j^*) \\ &+ \frac{1+\epsilon}{2}\frac{\Delta t}{(\Delta z)^2}\left[\eta\left(\frac{T_{j+1}^* + T_j^*}{2}\right)\frac{u_{j+1}^* + u_j^*}{2}\left(\frac{w_{j+1}^{n+1}}{u_{j+1}^*} - \frac{w_j^{n+1}}{u_j^*}\right)\right. \\ &\left.- \eta\left(\frac{T_j^* + T_{j-1}^*}{2}\right)\frac{u_j^* + u_{j-1}^*}{2}\left(\frac{w_j^{n+1}}{u_j^*} - \frac{w_{j-1}^{n+1}}{u_{j-1}^*}\right)\right] \\ &+ \frac{1-\epsilon}{2}\frac{\Delta t}{(\Delta z)^2}\left[\eta\left(\frac{T_{j+1}^n + T_j^n}{2}\right)\frac{u_{j+1}^n + u_j^n}{2}\left(\frac{w_{j+1}^n}{u_{j+1}^n} - \frac{w_j^n}{u_j^n}\right)\right. \\ &\left.- \eta\left(\frac{T_j^n + T_{j-1}^n}{2}\right)\frac{u_j^n + u_{j-1}^n}{2}\left(\frac{w_j^n}{u_j^n} - \frac{w_{j-1}^n}{u_{j-1}^n}\right)\right], \tag{B 12} \end{aligned}$$

$$\begin{aligned} T_j^{n+1} = T_j^n &- \frac{\Delta t}{2\Delta z}\frac{w_j^n}{u_j^n}(T_j^n - T_{j-1}^n) - \frac{\Delta t}{2\Delta z}\frac{w_j^{n+1}}{u_j^{n+1}}(\tilde{h}_{j+\frac{1}{2}} - \tilde{h}_{j-\frac{1}{2}}) \\ &+ \frac{H}{2\sqrt{u_j^n}}[T_{wall}^4 - (T_j^n)^4]\Delta t + \frac{H}{2\sqrt{u_j^{n+1}}}[T_{wall}^4 - (T_j^*)^4]\Delta t \\ &- \frac{St}{u_j^n}\left[\frac{w_j^n}{\sqrt{u_j^n}}\right]^m(T_j^n - T_a)\Delta t - \frac{St}{u_j^{n+1}}\left[\frac{w_j^{n+1}}{\sqrt{u_j^{n+1}}}\right]^m(T_j^* - T_a)\Delta t, \tag{B 13} \end{aligned}$$

where

$$\tilde{f}_{j+\frac{1}{2}} = w_j^n + \frac{\mathscr{A}\left(2\,(w_j^{n+1} - w_{j-1}^n),\,(w_{j+1}^{n+1} - w_j^n)\right)}{2},$$

$$\tilde{g}_{j+\frac{1}{2}} = \frac{[w_j^n]^2}{u_j^n} - \frac{1}{W}\,\sqrt{u_j^n} + \frac{\mathscr{A}(2\,x, y)}{2},$$

$$x = \left(\frac{[w_j^*]^2}{u_j^*} - \frac{1}{W}\,\sqrt{u_j^*}\right) - \left(\frac{[w_{j-1}^n]^2}{u_{j-1}^n} - \frac{1}{W}\,\sqrt{u_{j-1}^n}\right), \qquad \text{(B\,14)}$$

$$y = \left(\frac{[w_{j+1}^*]^2}{u_{j+1}^*} - \frac{1}{W}\,\sqrt{u_{j+1}^*}\right) - \left(\frac{[w_j^n]^2}{u_j^n} - \frac{1}{W}\,\sqrt{u_j^n}\right),$$

$$\tilde{h}_{j+\frac{1}{2}} = T_j^n + \mathscr{A}\left(2\,(T_j^* - T_{j-1}^n),\,(T_{j+1}^* - T_j^n)\right),$$

and the special function $\mathscr{A}(\cdot, \cdot)$ is used for flux limiting, and it is defined as

$$\mathscr{A}(x, y) = \begin{cases} x, & \text{if } x \cdot y \geqslant 0 \text{ and } |x| \leqslant |y|, \\ y, & \text{if } x \cdot y \geqslant 0 \text{ and } |x| > |y|, \\ 0, & \text{if } x \cdot y < 0. \end{cases} \qquad \text{(B\,15)}$$

Or in a more compact form, $\mathscr{A}(x, y)$ can be expressed as

$$\mathscr{A}(x, y) = \operatorname{sgn}(x) \max\left(0, \min(|x|, \operatorname{sgn}(x) \cdot y)\right). \qquad \text{(B\,16)}$$

In (B 12), ϵ is a free parameter between 0 and 1. If ϵ is 0, then one obtains the second-order Crank–Nicolson method; if ϵ is 1, then one has a complete implicit first order method.

References

[1] BURGMAN, J. A. (1970) Liquid glass jets in the forming of continuous glass fibers. *Glass Technology*, **11**(4), 110–116.

[2] BECHTEL, S. E., CARLSON, C. D. & FOREST, M. G. (1995) Recovery of the Rayleigh capillary instability from slender 1D inviscid and viscous models. *Physics of Fluids*, **7**, 2956–2971.

[3] BECHTEL, S. E., FOREST, M. G., WANG, Q. & ZHOU, H. (1998) Free surface viscoelastic and liquid crystalline polymer fibers and jets. *Advances in the Flow and Rheology of Non-Newtonian Fluids*, **B**, 1069–1116.

[4] BERIS, A. N. & LIU, B. (1988) Time dependent fiber spinning equations: 1. Analysis of mathematical behavior. *J. Non-Newtonian Fluid Mechanics*, **26**, 341–361.

[5] DEWYNNE, J. N., OCKENDON, J. R. & WILMOTT, P. (1989) On a mathematical model for fibre tapering. *SIAM J. Appl. Math.* **49**, 983–990.

[6] EGGERS, J. & DUPONT, T. F. (1993) Drop formation in a one-dimensional approximation of the Navier-Stokes equation. *J. Fluid Mech.* **262**, 205–221.

[7] FOREST, M. G. & WANG, Q. (1994) Dynamics of slender viscoelastic free jets. *SIAM J. Appl. Math.* **54**(4) 996–1032.

[8] FOREST, M. G. & ZHOU, H. (2001) *Models for Filaments and Fibers of Simple to Complex Liquids*. University of North Carolina Lecture Notes.

[9] FOREST, M. G., ZHOU, H. & WANG, Q. (2000) Thermotropic liquid crystalline polymer fibers. *SIAM J. Appl. Math.* **60**(4), 1177–1204.

[10] FOREST, M. G., ZHOU, H. & WANG, Q. (1999) A model study of the spinning of thermotropic

liquid crystalline polymers: Fiber performance predictions and bounds on throughput. *Advances in Polymer Technology*, **18**(4), 314–335.

[11] GEYLING, F. T. & HOMSY, G. M. (1980) Extensional instabilities of the glass fibre drawing process. *Glass Technology*, **21**(2), 95–102.

[12] GLICKSMAN, L. R. (1968) The cooling of glass fibres. *Glass Technology*, **9**(5), 131–138.

[13] HARTEN, A. (1987) High resolution schemes for hyperbolic conservation laws. *J. Computational Physics*, **135**(2), 260–278.

[14] HUYNH, B. P. & TANNER, R. I. (1983) Study of the non-isothermal glass fibre drawing process. *Rheology Acta*, **22**, 482–499.

[15] KASE, S. & MATSUO, T. (1965) Studies of melt spinning. I. On the stability of melt spinning. *J. Polymer Sci. A*, **3**, 2541–2554.

[16] LEVEQUE, R. J. (1992) *Numerical Methods for Conservation Laws*. Springer-Verlag.

[17] LIU, B. & BERIS, A. N. (1988) Time dependent fiber spinning equations: 2. Analysis of mathematical behavior. *J. Non-Newtonian Fluid Mech.* **26**, 363–394.

[18] MACCORMACK, R. W. (1976) A rapid solver for hyperbolic systems of equations (in aerodynamics). *Proceedings 5th International Conference on Numerical Methods in Fluid Dynamics*, pp. 307–17.

[19] MARCUSE, D. (1975) Radiation losses of the HE_{11} mode of a fiber with sinusoidally perturbed core boundary. *Appl. Optics*, **14**, 3021–3025.

[20] *Myers, M.* (1989) A model for unsteady analysis of preform drawing. *AIChE J.* **35**(4), 592–602.

[21] *Pearson, J. R. A.* (1985) *Mechanics of Polymer Processing*. Elsevier.

[22] PEARSON, J. R. A. & RICHARDSON, S. M. (1983) *Computational Analysis of Polymer Processing*. Elsevier.

[23] SCHULTZ, W. W. & DAVIS, S. H. (1982) One-dimensional liquid fibers. *J. Rheology*, **26**, 331–345.

[24] TING, L. & KELLER, J. B. (1990) Slender jets and thin sheets with surface tension. *SIAM J. Appl. Math.* **50**, 1533–1535.

[25] YOUNG, D. G. & DENN, M. M. (1989) Disturbance propagation in melt spinning. *Chem. Eng. Sci.* **44**(9), 1807–1818.

[26] YEH, C. (1990) *Handbook of Fiber Optics: Theory and applications*. Academic Press.